Microporous and Mesoporous Materials 225 (2016) 534–542

Contents lists available at ScienceDirect

Microporous and Mesoporous Materials

journal homepage: www.elsevier.com/locate/micromeso

Biotemplated synthesis of mesoporous silica for doxycycline removal. Effect of pH, temperature, ionic strength and Ca^{2+} concentration on the adsorption behaviour

Maximiliano Brigante [a, b, *], Marcelo Avena [a, b]

[a] INQUISUR, Departamento de Química, Universidad Nacional del Sur, Av. Alem 1253, 8000, Bahía Blanca, Argentina
[b] Consejo Nacional de Investigaciones Científicas y Técnicas (CONICET), Argentina

ARTICLE INFO

Article history:
Received 30 November 2015
Received in revised form
8 January 2016
Accepted 12 January 2016
Available online 3 February 2016

Keywords:
Mesoporous silica
Hydroxyethyl starch
Solid-water interface
Doxycycline adsorption
Cation-bridging

ABSTRACT

Mesoporous silica (SiO_2) materials were synthesized in acidic media, using tetraethyl orthosilicate as silica precursor and the water-soluble biopolymer hydroethyl starch (HES) as template, in order to evaluate the effect of temperature synthesis on the morphology and pore structure of synthesized materials. The results show that the mentioned parameters can be tuned by changing the temperature, i.e., from slices with worm-like mesopores of around 5 nm to microporous lamellas when the temperature synthesis increases from 60 °C to 100 °C, respectively. The changes are attributed to a (partial) degradation of the template that hinders the gel formation and disturbs its interaction with the silica species through H-bonds formations and/or electrostatic interactions. The synthesized solids were evaluated as adsorbent of the antibiotic doxycycline (DC) at several values of pH, temperature, ionic strength and Ca^{2+} concentration. The adsorption of DC strongly increases as pH and ionic strength decrease due to electrostatic attractions and H-bond formations between the functional groups of the antibiotic and the silica active sites. The presence of calcium ions strongly increases the adsorption of DC at pH > 4.4 due to the formation of ternary DC–Ca^{2+}–SiO_2 complexes by calcium-bridging. However, Ca^{2+} concentrations higher than 10^{-3} M cause the DC precipitation at pH 7 or higher. The analysis of thermodynamic parameters suggests that the adsorption of DC on SiO_2 is exothermic and spontaneous in nature. The effect of the tetracycline structure on the adsorption capacity of the synthesized material was also evaluated and discussed.

1. Introduction

Effective utilization of natural renewable resources has attracted increasing attention in recent years, and become an important aspect of green chemistry. However, only a low percentage of the produced biomass (mainly composed by polysaccharides) is used on the industry, the most decays and recycles along natural pathways [1]. In these circumstances, finding efficient applications that add supplementary value should represent one of the multidisciplinary research topics of this century beginning.

Among polysaccharides, starch has a special place due to its abundance, low-cost and properties derived from its two constituents, amylose and amylopectin. However, it is known that the solubility of starch in water is limited. Hydroxyethyl starch (HES) is a non-ionic starch derivate. HES consists in a large number of glucose units joined by glycosidic bonds in which some of the hydroxyl groups of the glucose are replaced by hydroxyethyl units provided by a substituent molecule (see in the Supplementary Material, SM, SM Fig. S1). This modification improves the solubility of starch in water, increasing the viscosity of the HES solution [2]. Among their applications, HES is one of the most frequently used plasma volume expander for hemodynamic stabilization, i.e., by replacing intravascular volume deficits with HES solutions, tissue perfusion can be improved and the development of multiple organ failures may be prevented [3].

In recent years, soluble starch derivates have also attracted considerable attention in material science and technology due to its application in the fields of the control of particle morphology [4], structure-directing agent [5], and carbonaceous nanoarchitecture

* Corresponding author. INQUISUR, Departamento de Química, Universidad Nacional del Sur, Av. Alem 1253, 8000, Bahía Blanca, Argentina. Tel.: +54 291 4595101x3593.
E-mail address: brigante@uns.edu.ar (M. Brigante).

http://dx.doi.org/10.1016/j.micromeso.2016.01.035
1387-1811/

source [6]. This is due to be a renewable, easily available (i.e., from native starch), relatively inexpensive and environmentally benign biopolymer if it is compared with the commonly surfactants used as template. In fact, it is believed that the calcination of quaternary ammonium salts derived templates during the synthesis of mesoporous materials could generate various organic amines compounds, NO_x, etc., greenhouse gas species that must be removed from the effluent for environmental reasons [7]. Moreover, it is known that the polysaccharide forms dynamic intra- or intermolecular supramolecular associations, establishing coordinative bonds with various transitional metal ions, a key role on the synthesis of metal oxides nanoparticles and on the remotion of heavy metal ions from surface and wastewaters [8,9].

The aim of this article is to present a study of the hydrothermal synthesis of mesoporous silica materials in acidic media by reaction of tetraethyl orthosilicate and HES, which act as silica precursor and template, respectively. Our research will therefore focus on the effect of the temperature on the structural and texture properties of the resulting materials. The adsorption capacity of obtained materials towards the antibiotic doxycycline was also evaluated. The data obtained at a variety of pH, temperature, ionic strength and Ca^{2+} concentration are used to gain insights into the mechanisms that govern the adsorption process and into the factors that promote or prevent adsorption. Mesoporous silica -and related materials- is known to be a promising candidate for tetracycline remotion as well as other pollutants from surface and waste waters due to its high surface area (>200 $m^2\ g^{-1}$, higher than metal oxides and oxyhydroxides), ordered pore distribution, narrow pore size distribution (pore width between 2 and >10 nm, higher than zeolites), high thermal stability and easy regeneration and reusability [10]. The obtained results will also serve as a basis for finding new and friendly templates for material synthesis.

2. Materials and methods

2.1. Chemicals

Tetraethyl orthosilicate (TEOS, 99%) and hidroxyethyl starch (HES, MW = 200,000 Da) were purchased from Aldrich. Potassium chloride, potassium hydroxide, potassium nitrate, calcium chloride, nitric acid, and hydrochloric acid were obtained from Anedra.

Doxycycline hydrochloride (DC) was purchased from PARAFARM. The structural formula of DC is shown in Fig. 1. In aqueous solutions three different groups of the molecule can undergo protonation–deprotonation reactions depending on the pH of the solution giving rise to the formation of three different species. The fully protonated species of DC exist at low pH values ($DCH_3^{\pm}$). As the pH increases, the first deprotonation step (pKa = 3.5) occurs at the hydroxyl group on C3 leading to the formation of zwitterionic species ($DCH^{\pm}$). The second deprotonation step (pKa = 7.7) involves the O10–O12 ketophenolic hydroxyl group giving rise to a specie with a negative charge (DCH^-). Finally, the third deprotonation (pKa = 9.5) involves the dimethylamino group giving rise to a specie with two negative charges (DC^{2-}) [11]. As comparative purposes, the other two tetracycline used in this work, tetracycline hydrochloride (TC) and minocycline hydrochloride (MC), were also obtained from PARAFARM. The molecular structure of both antibiotics and their speciation as a function of the pH can be found elsewhere [12].

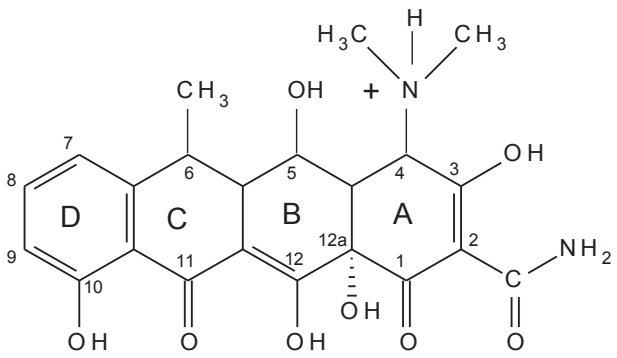

Fig. 1. Molecular structure of fully protonated DC.

All chemicals were of analytical grade and used as received. Doubly distilled water was used for the preparation of solutions.

2.2. Synthesis and characterization of mesoporous silica

Mesoporous silica (SiO_2) was synthesized as follows: 11.6 mL of TEOS were mixed with 2 mL of water and stirred in an autoclave flask for 10 min at 500 rpm. At the same time, 38 mL of 13 g L^{-1} HES solution were prepared by adding the desired amount of the soluble starch to water. This mixture was stirred in a conical flask to form a transparent template solution and then it was left at room temperature. To obtain the mesoporous material, 20 mL of a 1.38 M HCl solution were added drop by drop to the TEOS solution under stirring and 2 min later the HES solution was incorporated. The final pH of the mixture was around 0.4. The resulting gel was stirred for 5 min and then left for 48 h in an autoclave at 60 °C. After this, the gel was filtered and washed with distilled water and dried at room temperature. Finally, it was calcined in an air flux by increasing the temperature from room temperature to 540 °C with a heating rate of 2°C min^{-1}, and holding for 6 h at 540 °C. To evaluate the effect of temperature synthesis the gel was also left for 48 h in an autoclave at 100 °C. The obtained materials were named SiO_2-HES60 and SiO_2-HES100 in order to indicate the products synthesized at 60 °C and 100 °C, respectively.

The synthesized materials were characterized by the techniques usually employed in porous materials, such as scanning and transmission electron microscopy (SEM and TEM); XRD; FT-IR spectroscopy; electrophoretic mobility measurements; and the N_2-BET method for surface area, pore volume and pore diameter determination. SEM was performed using an EVO 40-XVP microscope. The samples were prepared on graphite stubs and coated with a ca. 300 Å gold layer in a PELCO 91000 sputter coater. TEM was performed using a JEOL 100 CX II transmission electron microscope, operated at 100 kV with magnification of 450,000×. Observations were made in a bright field. The powdered SiO_2 was placed on 2000 mesh copper supports. XRD patterns were obtained via a Philips PW 1710 diffractometer with CuKα radiation (λ = 1.5406 Å) and graphite monochromator operated at 45 kV, 30 mA and 25 °C; the angle step and counting time were 0.02°(2θ) and 1s, respectively. The electrophoretic mobility of SiO_2 was measured with a Zetasizer Nano Series instrument (Malvern Instruments Ltd.) at room temperature, and the Zeta potential was calculated using the Smoluchowski equation [13]. Stock suspensions containing 0.1 g L^{-1} of solid in 10^{-2} M KNO_3 were used for the measurements. The pH of the suspensions was adjusted to the desire value by adding small volumes of HNO_3 or KOH solutions. The N_2 adsorption isotherms at 77.6 K were measured with a Quantachrome Nova 1200e instrument. The samples were degassed at 373 K for 720 min at a pressure of 1×10^{-4} Pa. FT-IR experiments were recorded in a Nicolet FT-IR Nexus 470 Spectrophotometer. To avoid co-adsorbed water the samples were dried under vacuum until constant weight and then it was diluted with KBr powder before the FT-IR spectrum was recorded.

2.3. Adsorption experiments

Adsorption experiments (in darkness to avoid photodegradation) were obtained with a batch equilibration procedure using 15 mL polypropylene centrifuge tubes covered with polypropylene caps immersed in a thermostatic shaker bath. Before starting the experiment, a 2×10^{-3} M stock DC solution was prepared by adding the corresponding solid to water. Its pH was then adjusted to the desired value by adding HCl or KOH solutions. 20 mg of mesoporous material were introduced into the tubes and mixed with varying quantities of DC and KCl (used as supporting electrolyte) solutions. The range of initial DC concentration was 5×10^{-6}–1×10^{-3} M, and the final volume was 10 mL. The suspensions were then mixed on a rotator stirrer (FAES, Argentina) at 90 rpm for 6 h and the pH was checked and kept constant by adding small volumes (microliters) of concentrated HCl or KOH solutions. After equilibration, the phases into the tube were separated by centrifugation at 4000 rpm during 5 min and the supernatant was immediately analysed to quantify the adsorbate concentration (see below). Adsorbed DC was calculated from the difference between the initial DC concentration and the concentration of the antibiotic that remained in the supernatant solution. In most experiments no supporting electrolyte was used and the working temperature was 25 °C (except when effects of KCl and/or $CaCl_2$ concentration and temperature were investigated).

Quantification of DC was performed by UV-VIS spectroscopy at 275 nm for pH 4.4, at 274 nm for pH 7, and at 265 nm for pH 9.5 using an Agilent 8453 UV-VIS diode array spectrophotometer equipped with a Hellma 1 cm quartz cell. This is due to the shifting of the maximum absorption band of tetracycline antibiotics as pH varies [12]. The supernatant of the withdrawn aliquot was placed into the cell and the spectrum was recorded in the 200–900 nm wavelength range. Calibration curves at the working pH were conducted with several DC solutions having concentrations that ranged between 2×10^{-6} and 2×10^{-3} M. For comparative proposes, the adsorption of MC (maximum absorption wavelength $\lambda_{max} = 354$ nm) and TC ($\lambda_{max} = 358$ nm) were carried out at the same experimental conditions to DC. In adsorption experiments at several Ca^{2+} concentrations, the maximum absorption at 265 nm shifts to higher wavelengths as Ca^{2+} concentration increases due to the formation of water soluble metal-tetracycline complexes [14]. However, very good linearity in the calibration curves was found in all cases ($r^2 > 0.998$).

The adsorption isotherms were fitted using a Langmuir equation, which was commonly used in the adsorption of tetracycline antibiotics on several adsorbent systems [11,15]. The linear form of this equation is displayed as follows:

$$\frac{1}{DC_{ads}} = \frac{1}{q_{mon}} + \frac{1}{q_{mon} K_L DC_{eq}} \quad (1)$$

where DC_{ads} is the adsorbed amount of DC (μmol g^{-1}), DC_{eq} is the equilibrium concentration of DC in the supernatant (μM), q_{mon} is the maximum amount of antibiotic adsorbed (μmol g^{-1}) corresponding to complete coverage on the surface, and K_L is the Langmuir constant (μM^{-1}). From the linearized form of Eq. (1), q_{mon}, K_L and the correlation coefficient, r^2, can be calculated.

3. Results and discussion

3.1. General characteristics of the synthesized material

The morphology of the studied sample, whose particles have a characteristic white colouration, was investigated by SEM and TEM techniques and the respective micrographs are presented in Fig. 2. According to the SEM images, SiO_2-HES60 has smooth and plain slices with sandy granular aspect (Fig. 2a). At very high magnification (Fig. 2b), the sandy texture shows disordered worm-like mesopores, having a pore diameter of around 5 nm. SiO_2-HES100, on the contrary, shows a lamellar morphology (e.g. wrinkled sheets) without an appreciable sandy texture (Fig. 2c). According to the TEM image (Fig. 2d), the solid has not an apparent mesoporosity although the formation of micropores should not be discarded. Thus, the observed changes in morphology and pore structure suggest that the effect of the temperature synthesis on the template behaviour and its further interaction with the silica precursor was significant.

Fig. 3 shows the N_2 sorption isotherms of the studied samples. SiO_2-HES60 shows a typical type IV isotherm with H2 hysteresis loop, corresponding to a non-defined distribution of pore sizes and shapes, which appear in several inorganic oxide gels, glasses, and mesoporous silica as SBA-16 [16,17]. This was attributed in the past to “ink bottle pores”, but it is now recognized that this description provides an oversimplified picture of the actual situation, and that the role of network effects must be taken into account [18]. The well-defined step that occurs at P/P_0 between 0.5 and 0.8, corresponding to capillary condensation of N_2, indicates the uniformity of the pores, as shown from BJH pore size distribution (PSD) in the inset of Fig. 3. In fact, the pore radius was sharply distributed in a narrow range located at 2.4 nm (i.e., 4.8 nm pore width). As expected, the N_2 sorption isotherm of SiO_2-HES100 is a type I isotherm without an appreciable hysteresis loop. The shape of the sorption isotherm corresponds to materials with microporous structure or to solids with neither mesopores nor macropores [17], in agreement with TEM images. The calculated BET surface area and pore volume were 503 $m^2 g^{-1}$ and 0.564 $cm^3 g^{-1}$ for SiO_2-HES60, and 364 $m^2 g^{-1}$ and 0.138 $cm^3 g^{-1}$ for SiO_2-HES100, respectively.

From the PSD, it is not clear the formation of micropores in SiO_2-HES100, i.e., it shows a smooth shoulder in a pore radius of around 0.8 nm. This can be attributed to the fact that the BJH method can give erroneous results when the materials have pore width close to microporosity [19]. For materials with pore width higher than 3–4 nm, the BJH method is more accurate. In fact, a narrow -not a bimodal (e.g., micro and mesopores)- PSD is shown for SiO_2-HES60. A good alternative to confirm the no presence of micropores in this sample is in the use of theoretical o computational methods, such as nonlocal density functional theory (NLDFT) and/or Monte Carlo simulations. These tools can be powerful to predict the pore size of this kind of materials because they provide a more accurate structure of a fluid confined to narrow pores. For example, Ravikovitch et al. [19] showed a difference of around 1 nm in the calculated pore width by using BJH and NLDFT models when the solids (MCM-41 type silicas) have a pore width between 2 and 3.8 nm. The difference between models strongly decreases when the solids have a pore width of 4 nm or higher. The authors attributed this to the fact that (a) the BJH model underestimates the average pore when the material has pore sizes close to microporosity, and (b) the NLDFT model assumes a solid with ideal cylindrical pore structure.

To the best of our knowledge, there are no articles dealing about the assembly pathways between starch and/or starch derivates and the silica precursor for synthesizing a mesoporous material. On the one hand, starch species suffer gelatinization and retrogradation reactions in aqueous solutions due to the formation of multiple intermolecular hydrogen bonds between the hydroxyl groups of the starch molecules, present in both amylopectin and amylose units, and water [20]. Gelatinization (H-bond formations between amylopectin and amylose units in a 1:1 ratio) is also stimulated by decreasing the pH, by increasing the temperature or by the inclusion of species such as sodium silicate, proteins, dextrins, etc. [21].

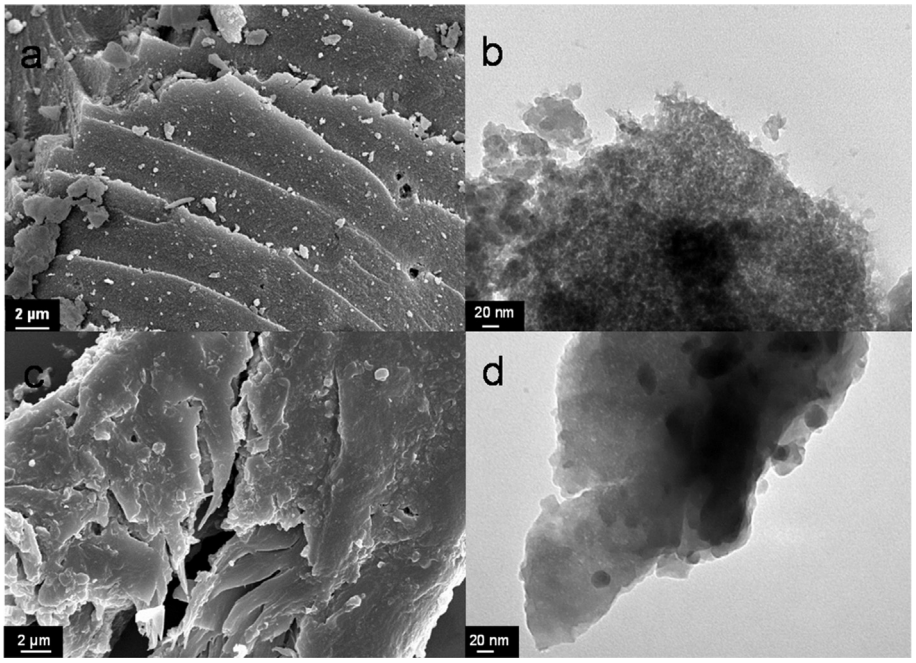

Fig. 2. Electronic micrographs of the synthesized samples: (a) SiO_2-HES60, SEM 10,000× (b) SiO_2-HES60, TEM 270000×; (c) SiO_2-HES100, SEM 10000×; and (d) SiO_2-HES100, TEM 270000×.

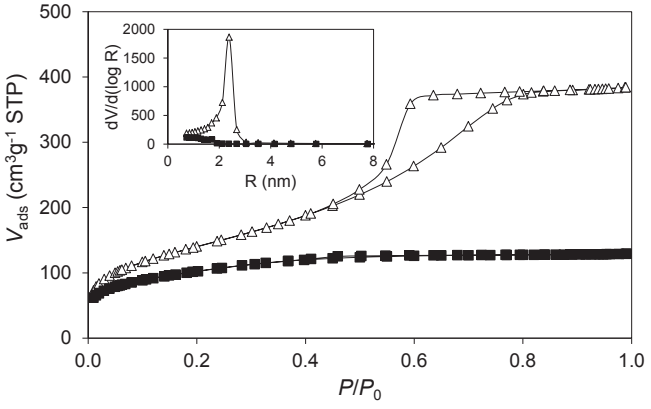

Fig. 3. Nitrogen adsorption–desorption isotherms of the synthesized samples: open triangles, SiO_2-HES60; and solid squares, SiO_2-HES100. The inset shows the BJH pore size distribution.

In the case of HES, El-Hinnawy et al. [22] have reported that the gelatinization occur at temperatures lower than the native starch and the retrogradation (i.e., H-bond formations between amylopectin and amylose in a 2:1 ratio) is minimized due to the partial substitution of hydroxyl groups by hydroxyethyl units. On the other hand, it is known that the hydrolysis of TEOS at pH < 2 tends to form protonated silica species (I^+). Such species can interact with non-ionic polymers, such as Pluronics, and the electrostatic assembly route is believed to be (N^0H^+) (X^-I^+), where N^0H^+ is the surfactant hydrogen bonded to a hydronium ion, and X^- is halide ion or counterion [23]. Thus, it is believed that the functional groups of HES interact with I^+ species by the same manner as the Pluronics. Once the hydrogel is formed, the TEOS suffers commonly polymerization and adsorption reactions to produce the silica matrix. Finally, the porous structure can be formed after the remotion of the HES hydrogel by calcination. Englin et al. [24] proposed an alternative mechanism using the biopolymer collagen as template. The authors revealed a high degree of replication of the collagen structure, with silica forming along the collagen fibrils through H-bonds formations and they concluded that the fine pore size in the final material is suggestive of the silica condensing around single helices of collagen. Although the formation of H-bonds between the functional group of HES and TEOS could be also important in the formation of SiO_2, Rashid et al. [21] reported that silicate species (as a sodium silicate) could interact with starch molecules by the formation C═O–O–SiO_2Na moieties through the amylopectin component.

It is also interesting to remark that both samples present significantly differences in texture and porous structure as shown in SEM and TEM images. This could be attributed to the partial degradation of the HES solutions at higher temperatures. Abbas et al. [25] demonstrated that degradation of HES generates species with lower MW (from 70,000 Da to 10,000 Da) and more soluble in water (up to 40%) when the temperature increases from 65 °C to 135 °C. At prolonged times the degradation can also generate side reactions (e.g. oxidation) that may result in the destruction of sugar molecules. This is confirmed by changing the colouration of the formed silica-HES hydrogel system after being hydrothermal synthesized at the two studied temperatures, i.e., from a white solid at 60 °C to brown ones at 100 °C. Autio et al. [26] reported that the oxidation of soluble starch molecules generates carboxylic and carbonyl groups which hinder the gel formation. Therefore, and although the formation of these functional groups might enhance the binding towards hydrophobic species (e.g., silica and/or organic silica precursors), the oxidation is undesirable due to the reduction of temperature at which gel-formation occurs and weakens the gels [25,26].

The results obtained by XRD, FT-IR spectroscopy and electrophoretic mobility are shown in the Supplementary Material (see SM Fig. S2a, S2b and S2c, respectively). The order (or not) in the porosity of SiO_2 and the pore symmetry is commonly analysed by XRD at lower 2-Theta angles (<10°). For example, SiO_2 materials with a MCM-41 type structure have three distinguishable peaks between 2° and 6°, (100), (110), and (200), which ascribe to a highly

ordered 2D hexagonal packing (*p6mm* symmetry) [10]. MCM-48 with a 3D cubic packing (*Ia3d* symmetry) have at least four discernible peaks at the same 2-Theta range related to the planes (211), (220) (420) and (332) [27]. SiO_2 materials with SBA-15 or SBA-16 type structures start having diffraction peaks at angles lower than 1° [23]. No distinguishable diffraction peaks are detected in both SiO_2-HES60 and SiO_2-HES100 in the 2°–6° range, i.e., it shows a broad peak commonly assigned to materials with non-ordered mesoporosity (e.g., worm-like porous structure) or with microporosity [28]. For such reason, the XRD spectra of the samples, shown in SM Fig. S2a, are similar. At higher angles, the solids show XRD patterns typical of amorphous materials, which are also characteristic of mesoporous silicas [29]. The mesoporous structures of SiO_2 are stable under our synthesis conditions and they do not collapse during calcination at 540 °C resulting in the transformation to the cristobalite phase [30]. This conversion causes two disadvantages: (a) materials with very low surface area and porosity and, thus, poor adsorption capacity; and (b) powders that cause chronic toxicity in humans and animals by air inhalation (e.g., lung cancer and silicosis) [31]. The most important features of the FT-IR spectra of both SiO_2 samples are: a broad band centered at around 3500 cm^{-1} associated to OH stretching of surface hydroxyls bound to silicon (Si–OH); a peak at 1640 cm^{-1} due to the OH bending mode of water molecules; a broad peak located at 1090 cm^{-1} with a shoulder at 1198 cm^{-1} which is attributed to asymmetric Si–O–Si vibrations; a peak centered at 804 cm^{-1} due to symmetric Si–O–Si vibrations; and peaks at 972 and 462 cm^{-1} assigned for Si–O–Si bending modes [32]. Finally, the Zeta potential vs. pH data shows that SiO_2-HES60 and SiO_2-HES100 have an isoelectric point of 2 and 2.8, respectively, which is in agreement with those reported in the literature [33], and references therein].

3.2. Adsorption studies

Adsorption isotherms of DC on the studied materials at 25 °C as a function of pH are shown in Fig. 4. The adsorption on SiO_2-HES60 is relatively high at pH 4.4 and decreases significantly at pH 7 and 9.5 (this last negligible) indicating that the affinity of DC for SiO_2 is higher at low pH. According to the data of the zeta potential vs. pH (see SM Fig. S2c), it is evident that the surface of SiO_2 at the experimental conditions should exhibit negative charges mainly due to the variable charge from pH dependent surface hydroxyl sites [34]. Thus, it is noted that the adsorbed amount of DC decreases as pH increases in response to: (a) the increasing number of negatively charged SiO_2 sites that are available due to the loss of H^+ from the surface [34], and (b) the increasing net negative charge of DC due to the deprotonation of the antibiotic. Both effects cause an increase of the electrostatic repulsion between DC and SiO_2.

Although the electrostatic interactions seem to be important in the adsorption of DC on SiO_2, non-electrostatic interactions between the organic species and the solid surface may play a significant role too [35]. These interactions, such as hydrogen bonding, surface complexation and van der Waals interaction are likely to operate not only with cationic species (DCH_3^+) but also with $DCH_2^{\pm}$ and DCH^- and they will contribute to the adsorption. This contribution also strongly decreases as pH increases.

The inset of Fig. 4a shows that the adsorption of DC on SiO_2 strongly depends on the experimental conditions in which the adsorbents were synthesized. In fact, the q_{mon} value for SiO_2-HES60 is 3-times higher than for SiO_2-HES100, and it is higher than for SiO_2 synthesized at 100 °C in an alkaline media (final pH = 11.8) by using commonly surfactants as template such as cetyltrimethylammonium bromide (CTAB) or the mixture composed by cetyltrimethylammonium p-toluene sulfonate or tosylate (CTAT) and Pluronic F68. The obtained results reveal that HES can be used as an alternative and environmental friendly structure-directing agent, and they confirm that the synthesis conditions, e.g., pH, temperature and type and concentration of used template play an important role on the morphology and on the reactivity of mesoporous silicas. In effect, the BET surface areas of SiO_2-HES60, SiO_2-CTAB:F68, SiO_2-HES100 and SiO_2-CTAB were 503 $m^2\ g^{-1}$, 468 $m^2\ g^{-1}$, 364 $m^2\ g^{-1}$ and 238 $m^2\ g^{-1}$, respectively, in agreement with the order of adsorption capacity at pH 4.4.

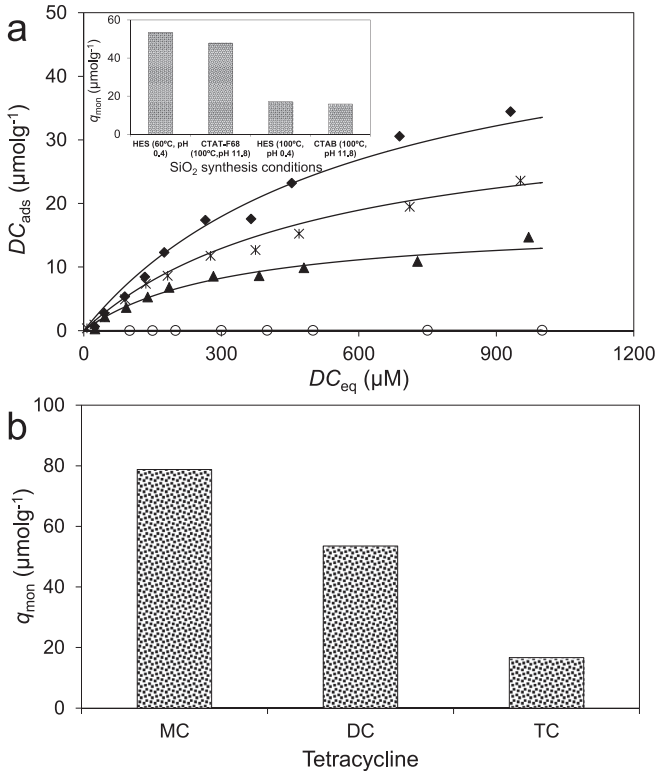

Fig. 4. (a) Effect of pH on the adsorption of DC on SiO_2-HES60. pH values: solid diamonds, pH 4.4; slashes, pH 7.0; and open circles, pH 9.5. Solid triangles show the adsorption of DC on SiO_2-HES100 at pH 4.4. Lines show predictions of Eq. (1). The inset shows the q_{mon} values obtained from adsorption isotherm at pH 4.4 as a function of the experimental conditions used for SiO_2 preparation. (b) Effect of the tetracycline structure on q_{mon} at pH 4.4.

Fig. 4b shows the effect of the chemical structure of the adsorbate on the q_{mon} value of SiO_2-HES60 at pH 4.4 and 25 °C. As expected, the adsorption of MC on SiO_2 was higher than DC and TC. At pH 4.4, MC forms a monovalent cation whereas DC and TC are mainly present in aqueous solution as a zwitterionic (in a 90–95%) [11,12]. Therefore, the interaction between MC (as MCH_3^+) and the silanol groups present in SiO_2, mainly driven by electrostatic interactions, is higher than in DC and TC. The major adsorption capacity of SiO_2-HES60 towards DC in comparison to TC can be attributed to the higher content of cationic species at the studied pH, i.e., the DC has a $pK_a = 3.5$ and TC has a $pK_a = 3.3$.

The binding between the antibiotic and silica can be visualized comparing the FT-IR spectra of DC and DC adsorbed on SiO_2-HES60 at pH 4.4 as shown in Fig. 5. DC shows characteristic absorption peaks between 3500 and 2700 cm^{-1} assigned to O–H and N–H stretching frequencies of alcohols and amines (NHR_3^+ groups), 1668 cm^{-1} assigned to the Amide I and Amide II bands, 1616 cm^{-1} and 1580 cm^{-1} assigned to C=O stretching vibration at rings A and C respectively, 1461 cm^{-1} assigned to C–C stretching vibration, 1360 cm^{-1} assigned to $-CH_3$ deformation vibration, 1244 cm^{-1} which is attributed to C–N amine stretching vibration, and 1175 cm^{-1} assigned to the phenolic C–O stretching band [36]. Silica

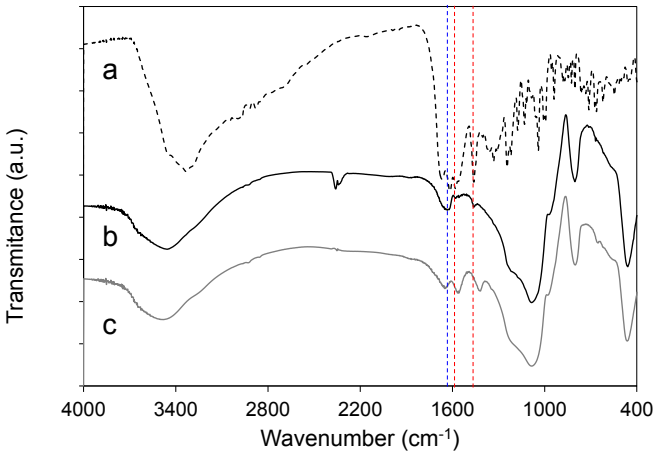

Fig. 5. FT-IR spectra of: (a) DC, (b) SiO_2-HES60, and (c) DC adsorbed on SiO_2-HES60 at pH 4.4.

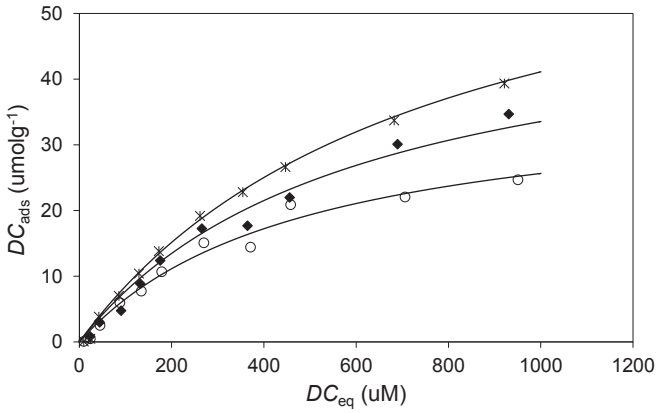

Fig. 7. Effect of temperature on the adsorption of DC on SiO_2-HES60 at pH 4.4. Temperatures: slashes, 45 °C; solid diamonds, 25 °C; and open circles, 5 °C. Lines show predictions of Eq. (1).

peaks were observed in the FT-IR spectrum of DC-SiO_2, whereas the bands assigned to the amine group were not observed. The peaks assigned to the polar groups of the antibiotic were shifted to lower frequencies with respect to bulk DC. The obtained results confirm that the NHR_3^+ groups of DC bind to the silica surface, mainly due to electrostatic interactions, whereas other polar groups of the molecule (amide, carbonylic and phenolic groups) could participate in non-electrostatic interactions (e.g. H-bond formations) with the surface.

The effects of ionic strength on the adsorption of DC isotherms on SiO_2-HES60 at pH 4.4 and 25 °C are shown in Fig. 6. The adsorption depends on the ionic strength; it decreases as the KCl concentration increases. These results suggest that formation of ionic pairs or outer–sphere complexes is the prevailing adsorption process: the competition between DC (as DCH_3^+ and/or $DCH_2^\pm$) and K^+ for negatively charged groups leads to an important decrease in DC adsorption by increasing KCl concentration. Results resemble those reported by Gao et al. [11] for the adsorption of DC on graphene oxide, where competition between the antibiotic and electrolyte cations was proposed to play a key role.

The effects of temperature on the adsorption of DC on SiO_2-HES60 at pH 4.4 are shown in Fig. 7. The adsorption is significantly affected by varying the temperature from 5 to 45 °C, i.e., the adsorption increases as temperature increases. Several reports exist about the effect of temperature in the adsorption behaviour of tetracycline-type antibiotics on different adsorbents. Tanis et al. [15] reported that the adsorption of TC on iron oxides-coated quartz increased by increasing temperature suggesting that a chemisorption-like process may play an important role in the tetracycline-adsorbent system. These observations are significantly different from those reported by Turku et al. [37], who showed that the adsorption of this antibiotic on silica decreased by increasing temperature (physical adsorption). Although the results presented in Fig. 7 seem to agree with those reported by Tanis et al. [15], the negative adsorption by increasing the ionic strength suggests that there is a physical adsorption in our system.

From the data showed in Fig. 7 the thermodynamic parameters Gibbs free energy (ΔG°), enthalpy (ΔH°), and entropy (ΔS°) for the adsorption of MC on the studied materials are obtained by using the following equations:

$$\Delta G^\circ = -RT \ln K, \tag{2}$$

$$\ln K = \frac{\Delta S^\circ}{R} - \frac{\Delta H^\circ}{RT}, \tag{3}$$

where K is the equilibrium constant, T is the absolute temperature, and R is the gas constant. The Langmuir isotherm can be applied to calculate the thermodynamic parameters assuming that $K = K_L$. ΔH° is obtained from van't Hoff plots as ln K_L versus $1/T$. The thermodynamic parameters are shown in Table 1. Chemisorption and physisorption are sometimes classified by the magnitude of the enthalpy change. When ΔH° is in the range of 30–70 kJmol^{-1}, the adsorption is considered to be chemisorption; i.e., a chemical bond is formed between the adsorbate and the surface [38]. When ΔH° is in the range of 0–10 kJmol^{-1}, the adsorption mechanism is considered to be physisorption; i.e., the bond between adsorbent and adsorbate is due to van der Waals interactions. This last seems to be occurring in our system. However, it is necessary to take into account that the above classification is commonly used to interpret adsorption at the solid–gas interface, which may significantly differ from the solid–liquid interface. For example, if a ligand exchange

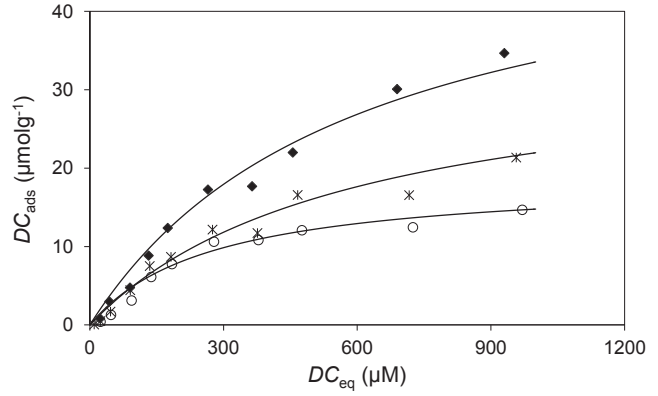

Fig. 6. Effect of ionic strength on the adsorption of DC on SiO_2-HES60 at pH 4.4. KCl concentrations: solid diamonds, 0 M; slashes, 0.01 M; and open circles, 0. 1 M. Lines show predictions of Eq. (1).

Table 1
Thermodynamic parameters of DC adsorption on SiO_2-HES60.

T (°C)	ΔG° (KJ mol^{-1})	ΔH° (KJ mol^{-1})	ΔS° (JK^{-1} mol^{-1})
5	−17.65		
25	−18.40	−8.06	34.56
45	−19.02		

reaction takes place between the adsorbate and the functional groups of the surface the ΔH° values could be negative, positive or even zero (with magnitudes up to 70 kJmol^{-1}) and still be a chemisorption reaction [39,40]. The negative value of ΔH° for the adsorption of DC on SiO_2 implies that the interaction of the antibiotic with the solid is an exothermic process. The positive sorption entropy indicates an increased randomness at the solid–water interface during DC adsorption [15]. Finally, the negative value of ΔG° at various temperatures shows that the nature of adsorption on SiO_2 is spontaneous under standard conditions.

The effects of Ca^{2+} concentration on the adsorption of DC on SiO_2-HES60 are shown in Fig. 8. The adsorption is significantly affected by varying the Ca^{2+} concentration from 0 to 10^{-3} M, i.e., the adsorption increases as Ca^{2+} concentration increases (Fig. 8a). This increase is mainly attributed to a calcium-bridging mechanism to form ternary DC–Ca^{2+}-SiO_2 complexes being the metal ion an active site for adsorption on SiO_2 [41]. The formation of calcium bridges was also reported by Bui and Choi [42] on the adsorption of ibuprofen and ketoprofen on SiO_2.

Although there are several reports about the complexation between tetracycline antibiotic with calcium and other metal ions in aqueous solution, the analysis of the stoichiometry of the formed complexes is strongly dependent on the nature of the tetracycline molecule. Such molecules contain electron-donor groups, mainly in N4–OH12a and O10–O12, that can form stable complexes with calcium and other metal ions [14,41,43]. In fact, Wessels et al. [44] reported that the coordination to the one or to another group is strongly dependent on the type of metal ion, i.e., Mg^{2+} coordinates to the dimethylamino–O3 site whereas Ca^{2+} coordinates to O10–O11 and O12–O1 sites. Parolo et al. [41] reported the formation of several and different water-soluble complexes between calcium ions and TC as a function of the pH and the Ca^{2+}: antibiotic molar ratio, i.e., the complexes $Ca(TCH)_2$, $Ca(TC)(TCH)^{-}$, $Ca(TC)_2^{2-}$ appear at pH > 6 for 1:1 M ratio, while the Ca_2TC^{2+} complex dominates the speciation at pH > 4.7 for 200:1 M ratio. No complexes were detected at pH 4.7 or lower. All formation constants (log K) of TC complexes with Ca^{2+} can be found elsewhere [41]. The authors also suggested that $Ca(TCH)_2$ and Ca_2TC^{2+} are the best candidates for adsorption on negative-charged montmorillonite at pH > 5. In the case of DC, the absence of the C6–OH group could cause a change in the binding characteristics, mainly in the protonation state of the complexes. This may indicate a different binding site of calcium ion to DC. In fact, Novák-Pékli et al. [45] reported the formation of $CaDCH^{+}$ species with log $K = 14.05 \pm 0.07$ through potentiometric titrations of a 1.5×10^{-4} M DC solution in presence of 5×10^{-4} M Ca^{2+}. Unfortunately, there is not information about the structure of the adsorbed species under these conditions. In all previous published articles, a rather simple electrostatic interaction is postulated, but it seems to be more complicated than that. However, it is clear from adsorption data that Ca^{2+} is playing a key role in promoting DC adsorption at pH 7.

Fig. 8a also shows that the removal amount of DC dramatically increases at 10^{-3} M Ca^{2+}. This could indicate that other removal processes, such as (surface) precipitation [43], play an important role in the DC-SiO_2 system. In fact, the precipitation was confirmed during the preparation of calibration curves at pH 7 and 10^{-3} M Ca^{2+}, i.e., a yellow solid was formed when the initial concentration of DC was 2.5×10^{-5} M or higher. The formation of the precipitate was also detected by comparing the FT-IR spectra of DC before and after interaction with 10^{-3} M Ca^{2+} with or without the presence of the SiO_2, as shown in Fig. 8b. Among the numerous differences between the FT-IR band assignments of DC and Ca–DC precipitate, it is distinguishable the no apparition of the band located at 1668 cm^{-1}, the shift of the 1616, 1580 and 1175 cm^{-1} bands to higher wavenumbers and the formation of new bands in the 1400–1500 cm^{-1} region. Similar bands are also shown in the ternary system which is indicative that most of DC is removed by precipitation and less by adsorption in such experimental conditions.

Fig. 9 shows the effects of a constant concentration of Ca^{2+} on the adsorption of DC on SiO_2 as a function of the pH. As expected, the adsorption decreases at pH 4.5 if it is compared with the same experiment performed in absence of Ca^{2+}. The no formation of complexes at pH 4.5 is indicative of competitive adsorption between DC and the metal ion by the active sites, such as shown in

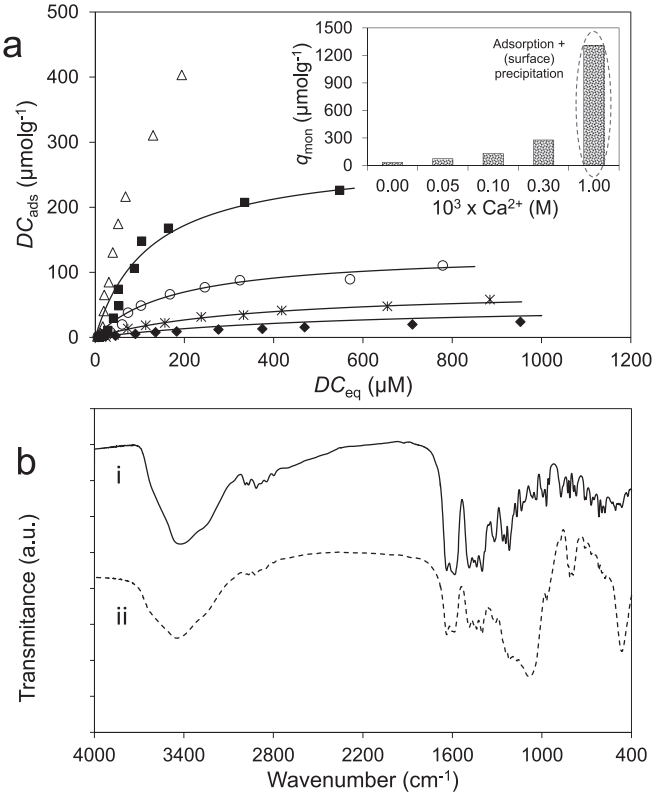

Fig. 8. (a) Effect of Ca^{2+} concentration on the adsorption of DC on SiO_2-HES60 at pH 7. Ca^{2+} concentrations: solid diamonds, 0M; slashes, 5×10^{-5} M; open circles, 10^{-4} M; solid squares, 3×10^{-4} M; and open triangles, 10^{-3} M. The inset shows the q_{mon} values obtained from respectively adsorption isotherms. Lines show predictions of Eq. (1). (b) FT-IR spectra of: DC–Ca^{2+} precipitate before (i) and after (ii) adsorption on SiO_2-HES at pH 7. Initial Ca^{2+} concentration = 10^{-3} M.

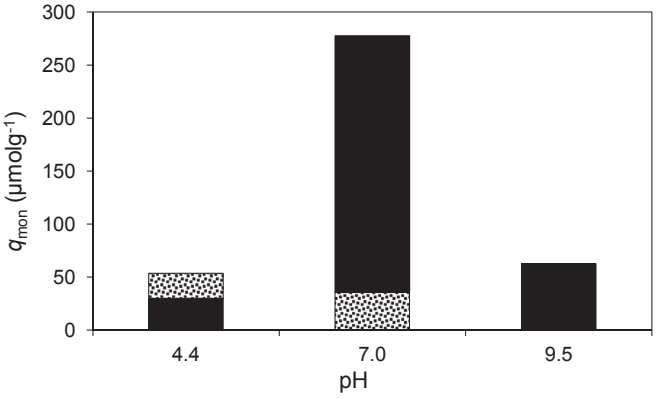

Fig. 9. Effect of the pH on q_{mon} values obtained from respectively adsorption isotherms in absence and in presence of 3×10^{-4} M Ca^{2+}.

Fig. 6. At pH > 4.5 the adsorption of DC increase, such as mentioned above, due to the formation of calcium bridges between DC and SiO_2. Similar effects on the adsorption by varying the pH and Ca^{2+} concentration were reported by Parolo et al. [41] on the adsorption of TC on Na-montmorillonite. The authors reported that at least two different adsorption processes took place in the studied systems, i.e., cation exchange and calcium-bridging. Cation exchange was the prevailing process at pH < 5, and thus, TC adsorption decreased by increasing total Ca^{2+} concentration. On the contrary, calcium-bridging was the prevailing process at pH > 5, and thus, TC adsorption increased by increasing Ca^{2+} concentration. As shown in Fig. 9, the cation bridging mechanism seems to be less favored at pH 9.5 than at pH 7 due to an increase of deprotonation of both DC and SiO_2 and an increase in the electrostatic repulsion between them.

In Figs. 4, 6–8 symbols correspond to data points whereas solid lines correspond to the best-fitting Langmuir isotherms calculated by adjusting the parameters q_{mon} and K_L. These parameters are listed in SM Table 1 for all experiments performed. Even though the formulated model is rather simple, it can fit reasonably well the adsorption of tetracycline antibiotics, i.e., the goodness-of-fit of Eq. (1) was checked through the r^2 values, which was between 0.96 and 1 in all cases. The last result is expected mainly because the Langmuir's theory assumes monolayer coverage of adsorbate over a homogenous adsorbent surface [10]. On the one hand, changes in all experimental conditions result in important changes in the adsorption isotherm, i.e., q_{mon} increases as temperature and Ca^{2+} concentration increase or as pH and ionic strength decrease. On the other hand, the maximum adsorption capacity on SiO_2 is around 278 μmol g^{-1} at pH 7 and 3×10^{-4} M Ca^{2+}, although the presence of calcium ions improve the adsorption at higher pH (up to three order of magnitude) if it is compared with the same experiments in absence of the metal ion.

4. Conclusions

The results shown in this article reveal that the use of the water-soluble biopolymer HES as template permit to obtain a mesoporous silica with worm-like pores. The temperature synthesis plays a key role on the gel formation and on the porosity mechanism of the synthesized products. At 60 °C silica with pores of around 5 nm are formed whereas at 100 °C the porosity and the surface area are strongly reduced due to the degradation of the biopolymer that hinders the gel formation. Electrostatic interactions and multiple H-bonds formations between the silica species and hydroxyl groups of HES seem to be responsible of the morphology and porous structure of the synthesized products.

From adsorption studies, it is interesting to remark that the adsorption of DC on the synthesized solids is intensely influenced by the surface area of the adsorbent and the chemical structure of the tetracycline antibiotic, and by varying experimental parameters such as pH, ionic strength, temperature and Ca^{2+} concentration. The adsorption is related to electrostatic attractions and H-bond formations between the functional groups of the antibiotic (e.g. quaternary ammonium, amide, phenols and carbonyls) and silica active sites. The presence of calcium ions strongly increases the adsorption of DC at pH > 4.4 due to the formation of ternary DC–Ca^{2+}-SiO_2 complexes by calcium-bridging. The analysis of thermodynamic parameters suggests that the adsorption on SiO_2 is exothermic and spontaneous in nature.

The obtained results have a significant importance in environmental processes, where polyvalent cations and other competing ions such as humic substances, phosphate, etc. [46] present in both surface- and wastewaters need to be considered while assessing the environmental fate and ecotoxicity of tetracycline antibiotics. The present results also permit to confirm that amorphous silicas with mesoporous structure are promising candidates for (a) ionic pollutants from aqueous solutions in environmental and engineering applications, and (b) tetracycline antibiotics in pharmaceutical applications, e.g., the formation of ternary tetracycline-Ca^{2+}-adsorbent material complexes could act as microbial inhibitors, drug delivery systems, etc.

Acknowledgements

This work was financed by SECyT-UNS (PGI UNS 24-Q051), CONICET (PIP 11220110100345) and ANPCYT (PICT 2011-1618). MB and MA are members of CONICET. The authors thank Dr. Marcelo Pistonesi (INQUISUR) for providing DC.

Appendix A. Supplementary data

Supplementary data related to this article can be found at http://dx.doi.org/10.1016/j.micromeso.2016.01.035.

References

[1] O. Carp, A. Tirsoaga, B. Jurca, R. Ene, S. Somacescu, A. Ianculescu, Carbohyd. Polym. 115 (2015) 285–293.
[2] K. Sommermeyer, F. Cech, B. Weidler, K. Henning, Hydroxylethyl, U.S. Pat. 5218,108, June 8, 1993.
[3] J. Boldt, Intensive Care Med. 35 (2009) 1331–1336.
[4] Y. Chen, J. Cao, M. Zheng, X. Ke, H. Ji, J. Liu, G. Ji, Chem. Lett. 35 (2006) 700–701.
[5] Y. Zhang, L. Hu, J. Han, Z. Jiang, Y. Zhou, Micropor. Mesopor. Mat. 130 (2010) 327–332.
[6] S. Yu, X. Cui, L. Li, K. Li, B. Yu, M. Antonietti, H. Colfen, Adv. Mater 16 (2004) 1636–1640.
[7] P.T. Tanev, T.J. Pinnavaia, Science 267 (1995) 865–867.
[8] M. Thirumavalavan, K.L. Huang, J.F. Lee, Colloid Surf. A 417 (2013) 154–160.
[9] A. Para, S. Karolczyk-Kostuch, M. Fiedorowicz, Carbohyd. Polym. 56 (2004) 187–193.
[10] M. Brigante, M. Avena, Micropor. Mesopor. Mat. 191 (2014) 1–9.
[11] Y. Gao, Y. Li, L. Zhang, H. Huang, J. Hu, S. Mazhar Shah, X. Su, J. Colloid Interface Sci. 368 (2012) 540–546.
[12] M. Brigante, P. Schulz, Chem. Eng. J. 191 (2012) 563–570.
[13] P. Leroy, C. Tournassat, M. Bizi, J. Colloid Interface Sci. 356 (2011) 442–453.
[14] Z. Zhang, K. Sun, B. Gao, G. Zhang, X. Liu, Y. Zhao, J. Hazard. Mat. 190 (2011) 856–862.
[15] E. Tanis, K. Hanna, E. Emmanuel, Colloid Surf. A 327 (2008) 57–63.
[16] P.I. Ravikovitch, A.V. Neimark, Langmuir 18 (2002) 9830–9837.
[17] J.M. Esparza, M.L. Ojeda, A. Campero, G. Hernández, C. Felipe, M. Asomoza, S. Cordero, I. Kornhauser, F. Rojas, J. Mol. Catal. A Chem 228 (2005) 97–110.
[18] K.S.W. Sing, D.H. Everett, R.A.W. Haul, L. Moscou, R.A. Pierotti, J. Rouquérol, T. Siemieniewska, Pure Appl. Chem. 57 (1985) 603–619.
[19] P.I. Ravikovitch, D. Wei, W.T. Chueh, G.L. Haller, A.V. Neimark, J. Phys. Chem. B 101 (1997) 3671–3679.
[20] M. Tako, Y. Tamaki, T. Teruya, Y. Takeda, Food Nutr. Sci. 5 (2014) 280–291.
[21] I. Rashid, M.H. Al Omari, S.A. Leharne, B.Z. Chowdhry, A. Badwan, Starch 64 (2012) 713–728.
[22] S.I. El-Hinnawy, H.M. El-Saied, A. Fahmy, A.E. El-Shirbeeny, K.M. El-Sahy, Starch 34 (1982) 112–114.
[23] D. Zhao, J. Feng, Q. Huo, N. Melosh, G.H. Fredrickson, B.F. Chmelka, G.D. Stucky, Science 279 (1998) 548–552.
[24] D. Eglin, G. Mosser, M.M. Giraud-Guille, J. Livage, T. Coradin, Soft Matter 1 (2005) 129–131.
[25] M.A. Abbas, S. Hameed, J. Kressler, Starch 65 (2013) 264–272.
[26] K. Autio, T. Suortti, A. Hamuned, K. Poutane, Carbohyd. Polym. 29 (1996) 155–161.
[27] K. Zhang, E.H. Yuan, L.L. Xu, Q.S. Xue, C. Luo, B. Albela, L. Bonneviot, Eur. J. Inorg. Chem. 2012 (2012) 4183–4189.
[28] T.R. Pauly, T.J. Pinnavaia, Chem. Mater 13 (2001) 987–993.
[29] W. Huang, X. Yu, J. Tang, Y. Zhu, Y. Zhang, D. Li, Micropor. Mesopor. Mat. 217 (2015) 225–232.
[30] G. Gu, P.P. Ong, C. Chu, J. Phys. Chem. Solids 60 (1999) 943–947.
[31] C.C. Leung, I.T.S. Yu, W. Cheng, Lancet 379 (2012) 2008–2018.
[32] K. Gude, V.M. Gun'ko, J.P. Blitz, Colloid Surf. A 325 (2008) 17–20.
[33] M. Kosmulski, J. Colloid Interface Sci. 353 (2011) 1–15.
[34] D.L. Sparks, Environmental Soil Chemistry, Academic Press, San Diego, CA, USA, 1995.
[35] G. Lagaly, M. Ogawa, I. Dékány, Clay mineral organic interactions, in: F. Bergaya, B.K. Theng, G. Lagaly (Eds.), Handbook of Clay Sciences, first ed., Elsevier, Oxford, 2006, pp. 309–377.

[36] C.F. Leypold, M. Reiher, G. Brehm, M.O. Schmitt, S. Schneider, P. Matousek, M. Towrie, Phys. Chem. Chem. Phys. 5 (2003) 1149–1157.
[37] I. Turku, T. Sainio, E. Paatero, Environ. Chem. Lett. 5 (2007) 225–228.
[38] F. Chen, C. Zhou, G. Li, F. Peng, Arab. J. Chem. (2012), http://dx.doi.org/10.1016/j.arabjc.2012.04.014 in press.
[39] D.P. Rodda, B.B. Johnson, J.D. Wells, J. Colloid Interface Sci. 184 (1996) 365–377.
[40] G. Sposito, The Surface Chemistry of Natural Particles, Oxford University Press, New York, USA, 2004.
[41] M.E. Parolo, M.J. Avena, G.R. Pettinari, M.T. Baschini, J. Colloid Interface Sci. 368 (2012) 420–426.
[42] T.X. Bui, H. Choi, Chemosphere 80 (2010) 681–686.
[43] J.J.R. Fraústo Da Silva, M.H. Mendoça Dias, Rev. Port. Quim 14 (1972) 159–169.
[44] J.M. Wessels, W.E. Ford, W. Szymczak, S. Schneider, J. Phys. Chem. B 102 (1998) 9323–9331.
[45] M. Novák-Pekli, M. E1-Hadi Mesbah, G. Pethó, J. Pharm. Biomed. Anal. 14 (1996) 1025–1029.
[46] P. Punamiya, D. Sarkar, S. Rakshit, R. Datta, Environ. Sci. Pollut. Res. 22 (2015) 7508–7518.